Pergamon

Cement and Concrete Research 32 (2002) 1331–1340

CEMENT AND CONCRETE RESEARCH

Modelling of a gas flow measurement Application to nuclear containment vessels

J. Verdier*, M. Carcassès, J.P. Ollivier

Laboratoire Matériaux et Durabilité des Constructions, INSA/UPS, 135 Avenue de Rangueil, 31077 Toulouse Cedex 4, France

Received 26 July 2001; accepted 13 March 2002

Abstract

The objective of this work is to simulate the gas flow across a concrete wall of a nuclear power plant internal enclosure. In the laboratory, permeability measurements are generally made on cylindrical samples (15 cm diameter×5 cm height: ϕ 15×5 cm) with a steady-state experiment. To be able to predict structural behaviour, we studied size effect and steady-state time with a modified CEMBUREAU permeability test. A statistical approach showed that there is no size effect on concrete permeability. Laboratory results found on cylindrical samples can be applied to tests in situ, where concrete specimens are thicker. A model based on the mass balance relation provided times to reach steady state and reproduced experimental flow kinetics for uniform water content across specimens.

Keywords: Concrete; Permeability; Steady state; Flow kinetics; Modelling

1. Introduction

The internal enclosures of nuclear power plants are built to resist to several accidents. The accidents considered lead to pressure and temperature increases inside the enclosure and vapour or air flow through the wall surface. That is why concrete walls must keep their full mechanical and airtightness characteristics throughout their lifetime to ensure security. We will not deal with the mechanical aspect in this paper. We will only study leaks due to the properties of the concrete. Security tests are carried out periodically to check wall airtightness. A security test consists of filling the reactor building (internal enclosure) with dry compressed air in pressure conditions that may occur during an accident. The flow rate is obtained from dry air weight loss calculations in the enclosed volume. The calculated mass flow leaving the enclosure from the internal side of the wall is the same as the mass flow leaving the external side only if the steady state has been reached. It is especially important to know the time to reach the steady state (TRSS) in nuclear power plant tests where the flow is measured upstream. Flows can be calculated from the concrete permeability. Indeed, if laws ruling fluid transport are applicable whatever the wall thickness, i.e. there is no size effect on permeability, then flows are directly proportional to permeability. The aim of this paper is to simulate in situ tests in order to predict the behaviour of concrete during a security test and the evolution of its leakage rate. The first part of the study discusses the size effect on permeability measurements. The study was conducted on dry samples. The second part deals with obtaining the TRSS. Because of its importance with regard to test measurements in situ, the influence of water content is also considered.

2. Material, mix proportions, curing and preconditioning

To conduct our experiments, a laboratory concrete was chosen to model the composition of a nuclear power plant concrete. We used the same cement, CPA-CEMI 52.5 R PMES CP2, and tried to obtain the same granular distribution. For this, a least-squares method was used to minimise the deviation between laboratory and in situ granular curves and to calculate mix proportions (Fig. 1). The use of local sand and gravel and the maximum gravel size used for our composition led to the only differences between the two

* Corresponding author. Tel.: +33-5-61-55-99-33; fax: +33-5-61-55-99-49.

E-mail address: verdier@insa-tlse.fr (J. Verdier).

0008-8846/02/$ – see front matter
PII: S0008-8846(02)00786-X

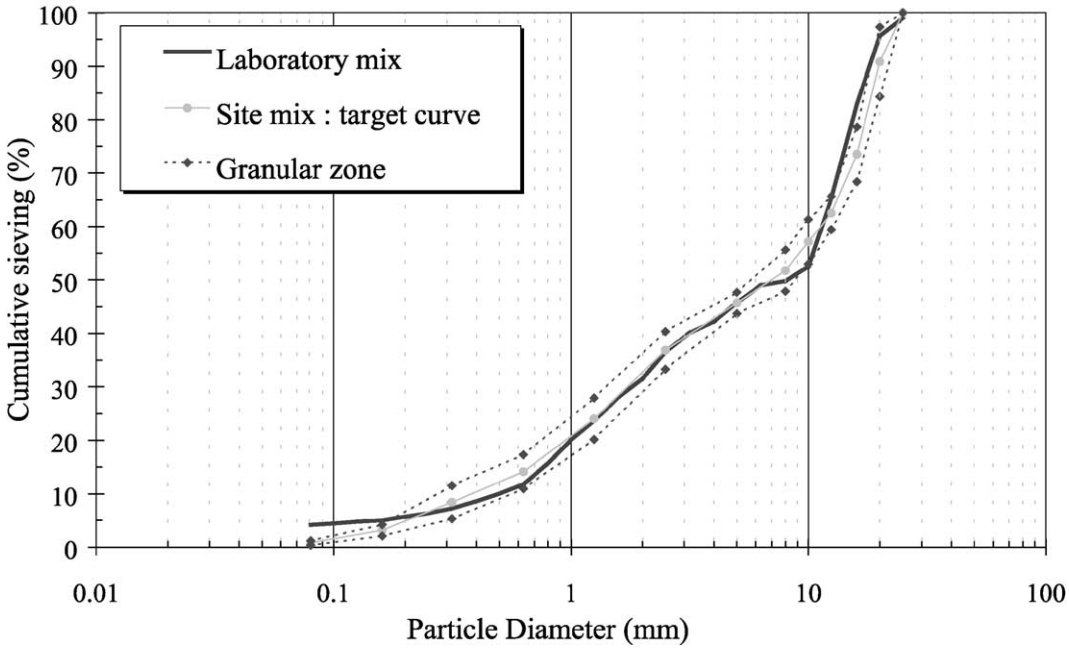

Fig. 1. Granular mix composition comparison of laboratory and site concrete.

compositions but the granular curves were similar (Fig. 1). The mix proportions for dry sand and gravel are given in Tables 1 and 2 for the power station and laboratory mixes, respectively. The mechanical and physical characteristics of the laboratory concrete were determined. Compressive strength and open water porosity tests were performed. The results and a comparison with site concrete are provided in Table 3.

Each cylindrical specimen used (ϕ 15×20 cm and ϕ 30×40 cm) was removed from its mould 24 h after casting and cured in water at a temperature of 20±2 °C for 28 days. After 21 days of curing, samples of various thicknesses (5 cm for the ϕ 15×20 cm and 5, 10, 20 and 30 cm for the ϕ 30×40 cm) were sawn from the original specimen and the first 25 mm of both sides were removed in an attempt to avoid skin effects. The thickness and diameter of each sample were precisely measured at eight points. Afterwards, samples were put back into the curing room. According to Powers' model, capillary porosity of a w/c=0.48 paste is disconnected after this curing [1]. The evolution of total porosity is due to hydration products. After 28 days of curing, the hydration is not achieved, but the curing time is sufficient to limit permeability variations due to evolution of the degree of hydration [2]. We therefore considered permeability to be time stabilised.

After 29 days, samples were placed in an oven and dried at 50 °C for 24 h, then oven-dried until their mass was constant at 80 °C for the ϕ 30 cm samples and at 105 °C for the ϕ 15 cm samples [3]. These 15-cm-diameter samples were used for the porosity measurements. Then permeability measurements in dry conditions were performed on them to analyse the statistical distribution of "permeability value" and to compare it with a theoretical model in order to use statistical methods to determine the size effect.

The samples used to determine the steady-state time for different saturation conditions (ϕ 15×5 cm) were subjected to another type of preconditioning. They were oven-dried at 50 °C to obtain a preassigned loss of water content. This

Table 1
Nuclear power plant composition and mix proportions

Component characteristics	Content in kg/m^3
Cement CPA HP PM	375
Site sand 0/0.8 mm	170
Site sand 0/0.6 mm	140
Site sand 0.8/5 mm	485
Site gravel 4/12 mm	340
Site gravel 12/25 mm	700
Water	180
BV 40 (superplasticizer)	1.5

Table 2
Laboratory composition and mix proportions

Component characteristics	Content in kg/m^3
Cement CPA-CEMI 52.5 R PMES CP2	375
Corrective local sand 0.63/1.25 mm	84.4
Corrective local sand 1.25/2.5 mm	67.9
Local sand 0/2.5 mm	473.4
Local gravel 2/6.3 mm	277.1
Local gravel 10/20 mm	932.2
Water	180
BV 40 (superplasticizer)	1.5

Table 3
Comparison of concrete characteristics

	28-day Compressive strength (MPa)	Attainable water porosity (%)
Site	50.3/63.3 (1 year)	13.5/14
Laboratory	62.3	13.2±1

temperature allows better control of the degree of saturation because of the drying process kinetics, which is slower. They were wrapped in adhesive aluminum foil and cling film for moisture conservation and were then put back in the oven for a time equal to the drying time in order to homogenise the moisture profile. The test was conducted after this period of water content equalisation. The moisture profile was assumed to be uniform throughout the sample.

After each drying period, as a precautionary measure, samples were thoroughly observed under a video microscope (150×) to detect or quantify the development of surface cracks. No visible crack initiation or propagation was detected in these periodical observations. Moreover, Abbas [4] found that all these different preconditioning temperatures had no influence on permeability values if specimens were in the same saturation conditions at the moment of the measurement. Yssorche et al. [5] report that the drying process, in these conditions, only leads to superficial microcracking, which does not reach the sample heart and has no influence on permeability measurements.

3. Permeability measurements

Permeability was measured with a constant head CEMBUREAU permeameter [6]. The standard apparatus and the one used for size effect analysis and for flow recording are illustrated in Fig. 2.

Upstream and downstream flows were measured with "mass flowmeters" and the volume flows at normal pressure and temperature conditions were calculated (expressed in normal litres per minute: nl/min). A data recording system (HP 34970 multimeter and PC) recorded the variation of the volume flow with time. For the size effect study, the permeability cell used for various sample thicknesses was adapted with Teflon blocks (Fig. 2). To be representative of a material, it is recommended that a permeability test be conducted on a minimum of three samples [7]. We followed this recommendation in all the experiments. We chose 1 MPa lateral confinement to ensure radial and ortho radial stresses of 1 MPa in the sample. These stresses are those that can be expected in a concrete wall for a test in situ at the end of the nuclear power plant's lifetime.

Gas permeability of porous media is generally obtained by determining the volume flow (Q_s) in a steady-state experiment. Permeability is given by the Hagen–Poiseuille relationship (Eq. (1)), using mass conservation in the steady state between the inner and outer sides of the sample. The flow is assumed to be laminar and unidirectional [6]. Theoretically, k_a is an intrinsic parameter.

$$k_a = \frac{2\mu L P_s Q_s}{A(P_e^2 - P_s^2)} \quad (1)$$

Here, μ (Pa s) is the dynamic viscosity of the fluid studied. L (m) is the sample thickness and A (m^2) is the section subjected to flow. P_e (Pa) is the upstream absolute pressure and P_s the downstream one. The only unknown parameter to be determined is the flow Q_s ($m^3\ s^{-1}$).

Actually, the apparent permeability k_a (m^2) depends on the pressure gradient, temperature, water saturation and material microstructure. The permeability given by Eq. (1) assumes a laminar flow, but, in fact, a nonviscous contribution due to the pore fineness in concrete is frequently observed (molecular

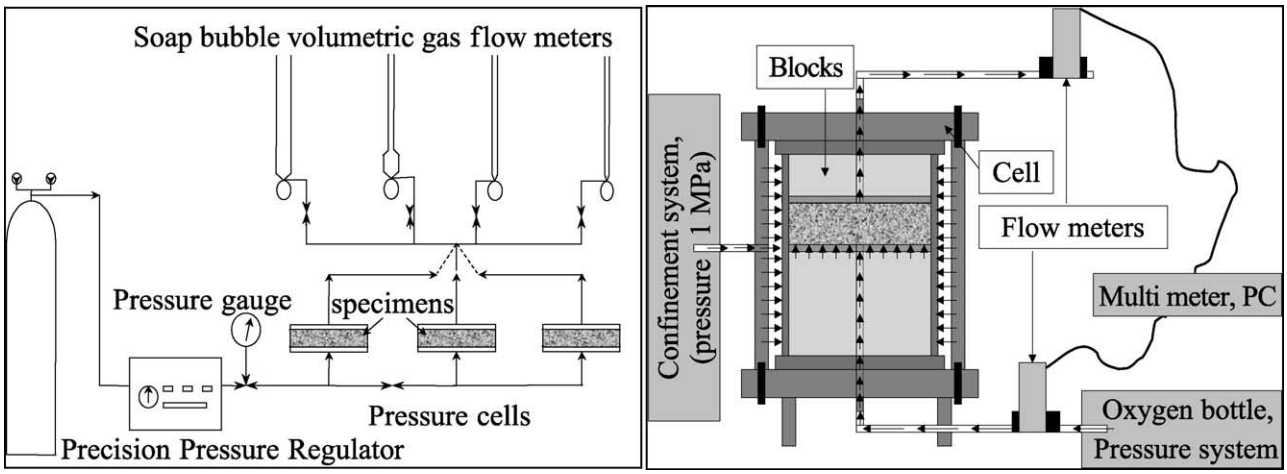

Fig. 2. Schematic layout of the experimental constant head permeameter.

effect and slipflow). These contributions and pressure dependence have been well known since Abbas et al. [8] proposed a law giving the "absolute" permeability k_i (Eq. (2)).

$$k_a = k_i\left[1 + \frac{\beta}{P_m}\right] \quad (2)$$

Here, P_m is the average pressure, $(P_e+P_s)/2$, and β is the Klinkenberg coefficient allowing nonviscous contributions to be estimated. Even so k_i is not really an "intrinsic" parameter because it depends on the water saturation. If we consider a given degree of water saturation of the material s, assumed to be uniform in the sample, k_a is called the apparent relative permeability because of the double dependence on pressure and water content.

4. Size effects on permeability

Perraton [7] showed that there was no diameter effect on permeability if the samples tested were similar in terms of

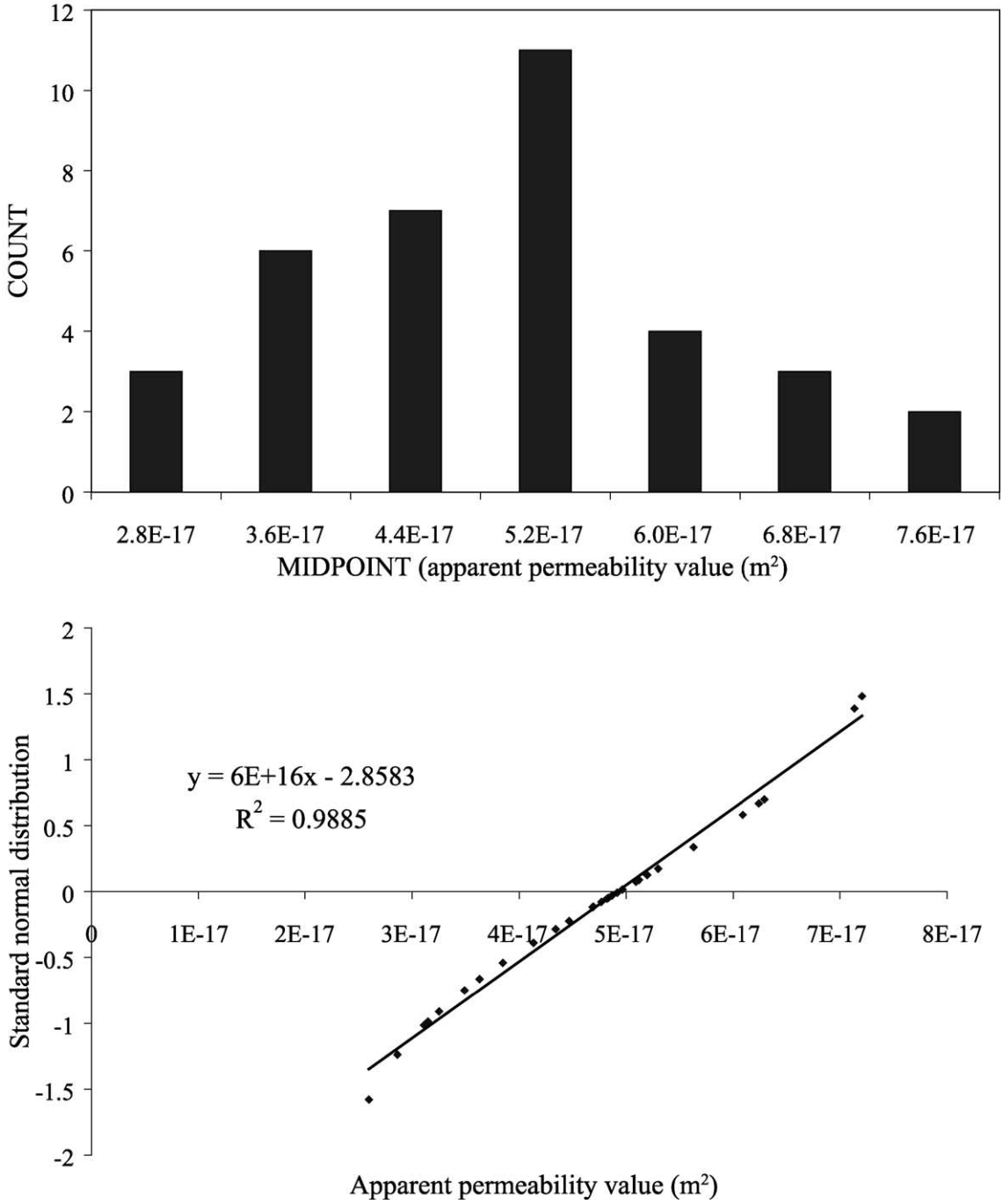

Fig. 3. Experimental distribution for apparent permeability values and Henry straight line (for a 0.4-MPa pressure gradient).

water content. To estimate the TRSS for walls of various thicknesses, we have to verify whether the apparent permeability of a dry sample is size dependent, using a probabilistic approach. First, we have to know the statistical distribution of permeability measured on dry samples of the same dimensions. If "permeability" follows a normal law (Gaussian distribution), we can analyse the influence of the thickness, obtained in dry conditions, by using a statistical approach.

A statistical analysis was carried out on a representative group of 36 apparent permeability values stemming from permeability tests on ϕ 15×5 cm samples for each head pressure (0.1, 0.2, 0.3 and 0.4 MPa). We supposed that the random variable "permeability" followed a normal law. A normal law is defined by a mean value (m) and a standard deviation (d). m and d were calculated from permeability measurement for the experimental distribution. We verified the hypothesis of a normal law with the Henry straight line. For each head pressure, the linear regression coefficient with the straight line was higher than 0.98. We give an example of the experimental distribution for a 0.4-MPa pressure gradient measurement in Fig. 3. We also verified some conformity criteria with the SAS software [9]. Shapiro–Wilk, Kolmogorov–Smirnov, Cramer–von Mises and Anderson–Darling tests indicated that statistical and theoretical distributions were close enough to conclude that permeability followed a normal law. P value was higher than .1 for each test [10].

Next, we verified the influence of thickness on permeability. The permeability results on 30-cm-diameter samples are given in Table 4. It gives the mean value (m) and the standard deviation (d) for the permeability measurements obtained at different pressure gradients. We compared independent specimen groups using a Fisher–Student's test on mean values. This was possible because of the Gaussian distribution of the permeability and because the variance of different sample series was sufficiently close. All thickness series were compared, and Fisher tests enabled mean values to be compared. This comparison led to the conclusion that the specimen groups were not different. This analysis was done with a 5% first-type risk. There was no size effect on permeability. So, the laboratory results could be transposed to in situ predictions.

Table 4
Apparent permeability mean values (m) and standard deviations (d) (10^{-17} m^2)

Sample thickness (cm)	Samples tested	Absolute applied pressure (MPa)							
		0.2		0.3		0.4		0.5	
		m	d	m	d	m	d	m	d
5	5	10.92	0.73	9.35	0.69	8.81	0.33	8.28	0.28
10	6	10.25	2.38	8.61	2.53	7.89	2.33	7.28	2.06
20	8	10.51	2.05	9.10	1.88	8.4	1.5	7.75	1.49
30	5	10.74	0.78	9.03	0.67	7.62	0.91	7.03	0.85

5. TRSS: development of a model

We knew from experimental results that the downstream pressure, where the flow was read, was close to atmospheric pressure. The apparent permeability measurement was performed when the outer flow value had become stabilised with time. At this time, up- and downstream mass flows were equivalent, and the pressure profile was fixed in the sample. The steady state had been reached. When the inlet pressure is initiated, the upstream mass flow decreases as the downstream flow increases. To describe the non-steady-state regime and to calculate the TRSS, we had to solve a differential equation given by the mass balance equation (Eq. (3)). This equation, written at a local level, is valid for any fluid. It expresses the fact that the variation of concentration with time at a material point is proportional to a flow divergence through the elementary surface around the volume considered. To represent the phenomenon on a macroscopic scale, we assume the medium to be a continuum, and we define a representative elementary volume in which macroscopic parameters are obtained from an average microscopic value [11].

$$\frac{\partial \rho\varphi}{\partial t} = -\nabla\rho \cdot \vec{u} \tag{3}$$

Where ρ is the gas (i.e. oxygen) density, and φ is the gas attainable volume porosity. φ is given by (φ=$\varphi_g(1-s)$), where φ_g is the total water porosity, and s is the degree of saturation. $\vec{u}$ is the fluid velocity given by Darcy's law (Eq. (4)). For a gas, the gravity term can be neglected in Eq. (4). The Hagen–Poiseuille expression (Eq. (1)) gives the apparent permeability value k_a.

$$\vec{u} = -\frac{k_a}{\mu}\,\mathrm{grad}(P + \rho g z) \tag{4}$$

We assimilate oxygen to a perfect gas since, in these pressure and temperature conditions, its compressibility factor is close to 1 [12]. Mariotte's law (Eq. (5)), which gives the relation between density and pressure, can be applied.

$$\frac{P}{\rho} = \frac{RT}{M} \tag{5}$$

Combining Eqs. (3)–(5) gives the time and space dependency of the pressure (Eq. (6)). In this expression, we consider that the average pressure is equal to the local pressure. This expression does not lead to an easy analytic solution, and it was solved using a finite difference method.

$$\left(\frac{\partial P}{\partial x}\right)^2 + P\frac{\partial^2 P}{\partial x^2} = \frac{\mu\varphi}{k}\frac{\partial P}{\partial t} \tag{6}$$

The finite difference method consists of expressing the derivatives of a function as the function's differences on a finite interval. Indeed, the derivative of a function $y(x)$ is the limit when Δx tends toward zero of the value increase

$[y(x+\Delta x)-y(x)]$ over an increase Δx of the independent variable. When Δx does not tend toward zero, derivatives are given by finite difference expressions. Of course, in this representation, an error occurs each time due to this derivative expression. This error can be estimated with a Taylor serial development of $y(x+\Delta x)$. The smaller Δx, the more accurate the calculated result of the function. We used the second order in our simulation, attempting to minimise this error. To represent the experiment as correctly as possible, we chose a stopping criterion based on an experimental test. Resolving the simulation to an absolute numerical solution goes much farther than the variations detectable in the experiment.

The solution validity of the simulation can be verified. The pressure function can be expressed in the steady state because, at this time, the pressure in the sample no longer varies with time. The left term of Eq. (6) is equal to zero, and the equation has an analytic solution given by Eq. (7).

$$P(x) = \sqrt{\frac{P_s^2 - P_e^2}{L}x + P_e^2} \tag{7}$$

We can conclude that, in the steady state, the pressure profile is independent of the material characteristics.

6. Results of modelling

6.1. Dry samples

First, we will give a representative example for a (ϕ 15×5 cm) dry sample. Experimentally, for a given pressure gradient, the variation of downstream volume flow with time was obtained with the data recorder (Fig. 4). The initial volume flow peak seen on experimental curves at the beginning of the measurement is due to the initiation of the inlet pressure. Apparent permeability was calculated from Eq. (1). This value was an input parameter of the simulation. The other inputs were the time and space steps, thickness and diameter of samples, porosity and pressure head. Boundary pressure conditions were given on the sample surface (first node) and the rest of the sample was assumed to be at the atmospheric pressure (other nodes) at the initial time. To stop the simulation and to compare modelling and experiments, we used a criterion based on the volume flow, in relation with the experimental accuracy. AFPC-AFREM [3] advocates stopping data measurement when the flow variation in a 15-min interval is lower than 3%. With our recording data, we had a better resolution, but we could not detect relative flow variations of less than 0.5% between two distinct periods separated by 10 min. Thus, we chose this criterion to stop the simulation program. Flows were computed on a space step with Eq. (1). We supposed that the steady state was obtained between two successive nodes. When the ratio between downstream flows computed at time t and at time $t-\Delta t$, related to the $t-\Delta t$ flow value, was lower than 0.5%, the steady state was assumed to have been reached. Of course, this Δt had to be sufficient to permit a downstream flow evolution between two measurement periods and had to correspond to the experimental stopping criterion. We considered that a 10-min Δt satisfied to this requirement. For a 5-cm sample, simulation results were close to the experimental data whatever the sample.

Fig. 4 shows experimental (exp) and simulated (theo) downstream flows versus time for three different head pressures. TRSS' are given in Table 5. In the range inves-

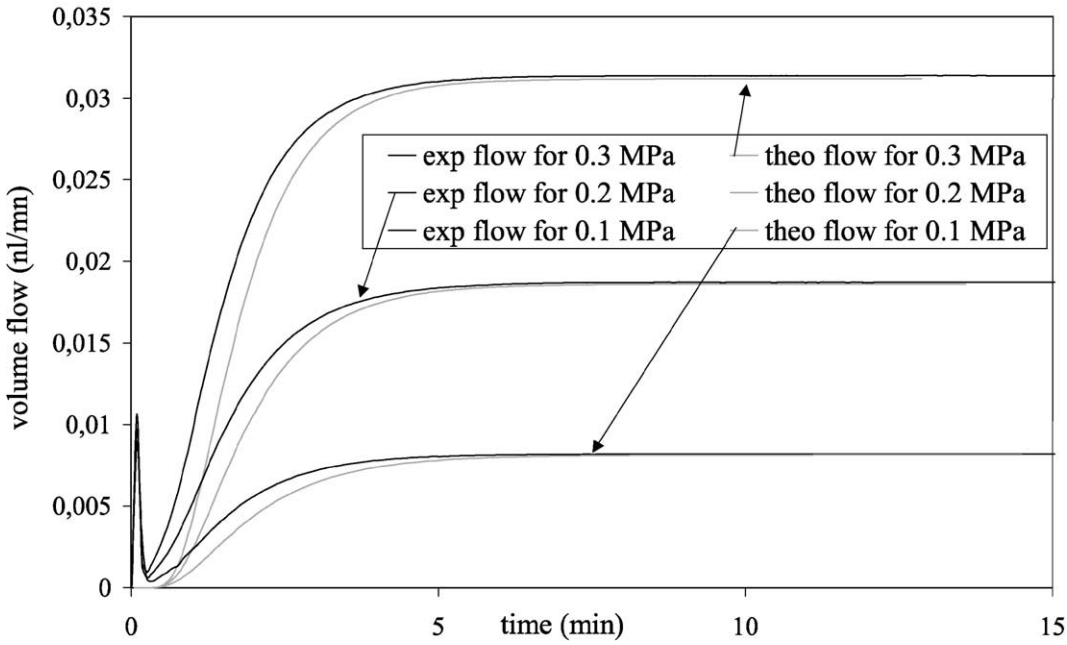

Fig. 4. Comparison between downstream flow kinetics for a ϕ 15×5 cm dry sample.

Table 5
TRSS (min) results and deviation, D (%), between theory and experiment

		Absolute head pressure (MPa)								
		0.2			0.3			0.4		
Thickness (cm)	Saturation	Exp	Theo	D (%)	Exp	Theo	D (%)	Exp	Theo	D (%)
5	dry	12	11.7	2.5	10.1	9.5	6	9.7	9.5	2

Table 6
TRSS (min) results and deviation, D (%), between theory and experiment

		Absolute head pressure (MPa)					
		0.2			0.5		
Thickness (cm)	Saturation (%)	Exp	Theo	D (%)	Exp	Theo	D (%)
5	10	11.1	11.4	2.6	8.2	8	2.5
	35	22.1	22.8	3	18.7	19.4	3.6
	53	23.9	24.9	4			
	79	34.7	36.7	5.5	30.6	28.5	6.9
10	dry	26.7	25.7	3.8	21	19.8	5.7
20	dry	58	71	18.4	51	53.3	4.3
30	dry	119	121	1.9	108	116	6.9

tigated, pressure had very little influence on the TRSS. This influence increased with the sample thickness. A comparison between pressure profiles at the steady-state time, calculated by Eq. (7) (theo) and simulated (sim) are shown on Fig. 5. The two curves are similar, and the chosen criteria allowed the theoretical profile to be reached. The simulation for dry samples was representative for the TRSS and reproduced flow kinetics correctly.

6.2. Percolation effects

Fig. 5 presents flow kinetics results for each thickness and for a 0.4-MPa pressure gradient. Tables 5 and 6 give the comparison between experimental and theoretical TRSS. D is the deviation between the two values, expressed as a percentage. Experimental and theoretical times are very close, but a difference remains between flow kinetics (Fig. 6). This difference increases with the sample thickness. Indeed, the model considers the material to be homogeneous and does not take into account the pore distribution in the porous network. So the occurrence of percolation preferential paths is not well reproduced in the model. Experimentally, the porosity does not completely participate in the flow, whereas in the model, all the porosity is considered in the flow.

To illustrate this percolation effect, we simulated a test for a 30-cm-thick sample submitted to a 0.1-MPa pressure gradient through its 0.07-m^2 apparent cross section. The sample was modelled as a composite material with two different components:

Component 1 represented 90% of the cross section (i.e. 0.063 m^2) with an apparent permeability, k_1, of 1×10^{-16} m^2.
Component 2 represented 10% of the cross section (i.e. 0.007 m^2) with an apparent permeability, k_2, of 3×10^{-16} m^2.

These two parts had the same total porosity and the same thickness as the initial specimen. For each component, we could calculate the downstream flow (Fig. 7, Curves 1 and 2

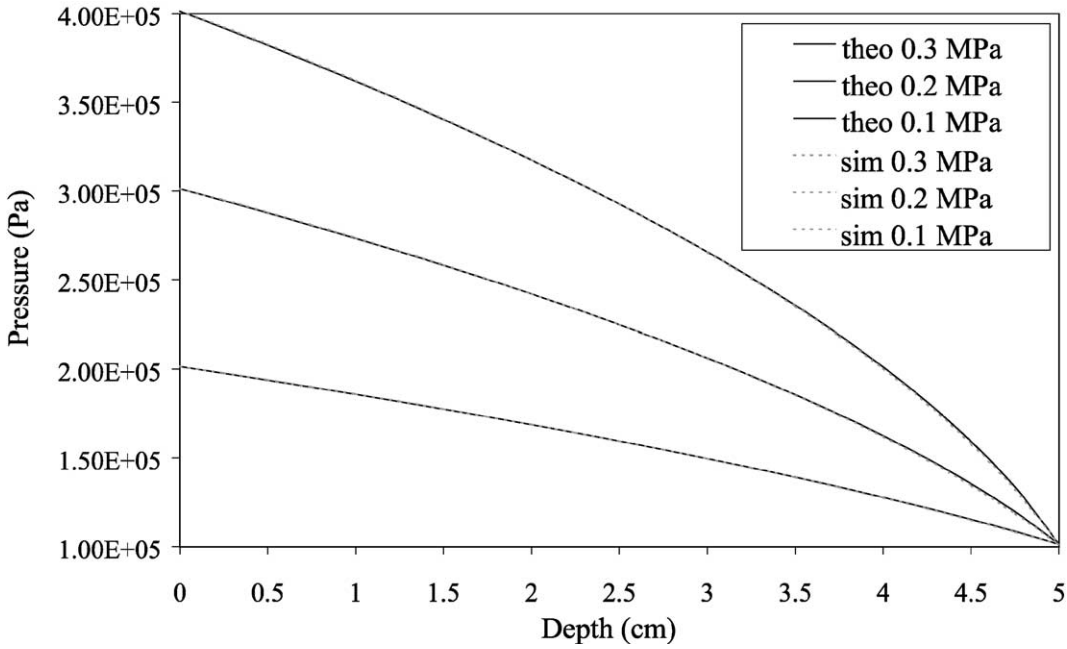

Fig. 5. Pressure profile in a 5-cm-thick sample in steady-state flow conditions.

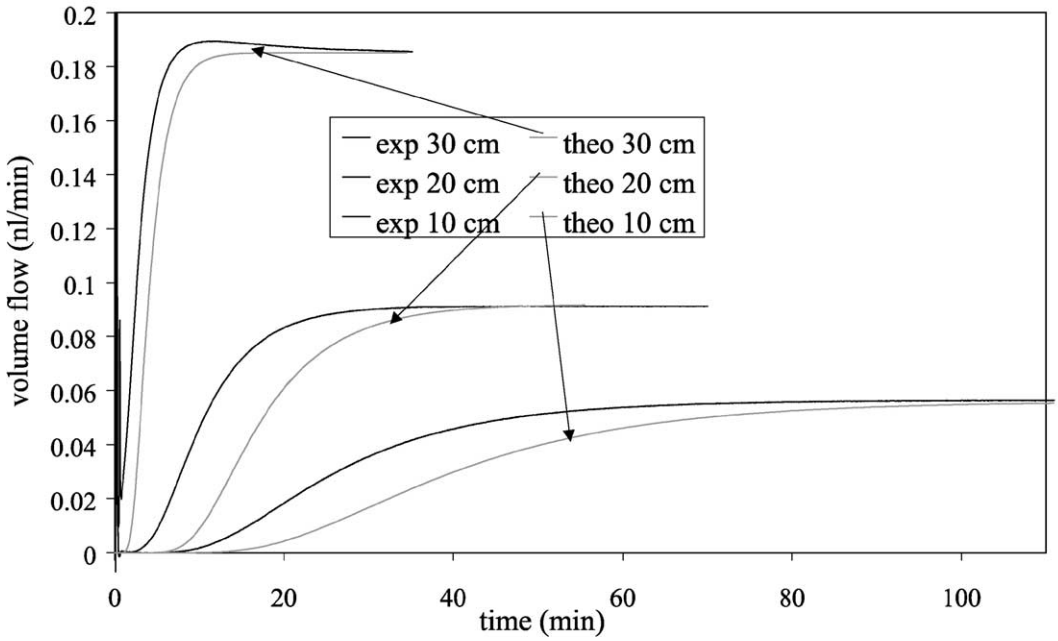

Fig. 6. Comparison between downstream flow kinetics for a 0.4-MPa pressure gradient.

for Components and 1 and 2). The sum of these two flows represents the flow across the whole specimen (Curve 3). The percolation depended only on the more permeable component. It is easy to understand that if we met these properties experimentally, the sum of downstream flows would be conditioned by the higher permeability because the fluid would come out faster in this case. From steady-state flow (curve 3), we calculated the apparent permeability k_a applying Eq. (1) (k_a=1.18×10^{-16} m^2). We simulated a test with this value for a whole specimen (Curve 4). We notice that the model does not take into account percolation preferential paths. Simulated Curve 4 is shifted in time with respect to Curve 3 (Fig. 7). The model does not distinguish the different permeability areas. The input of the model ''apparent permeability value'' (obtained from a flow value in a steady-state experiment) represents a global parameter

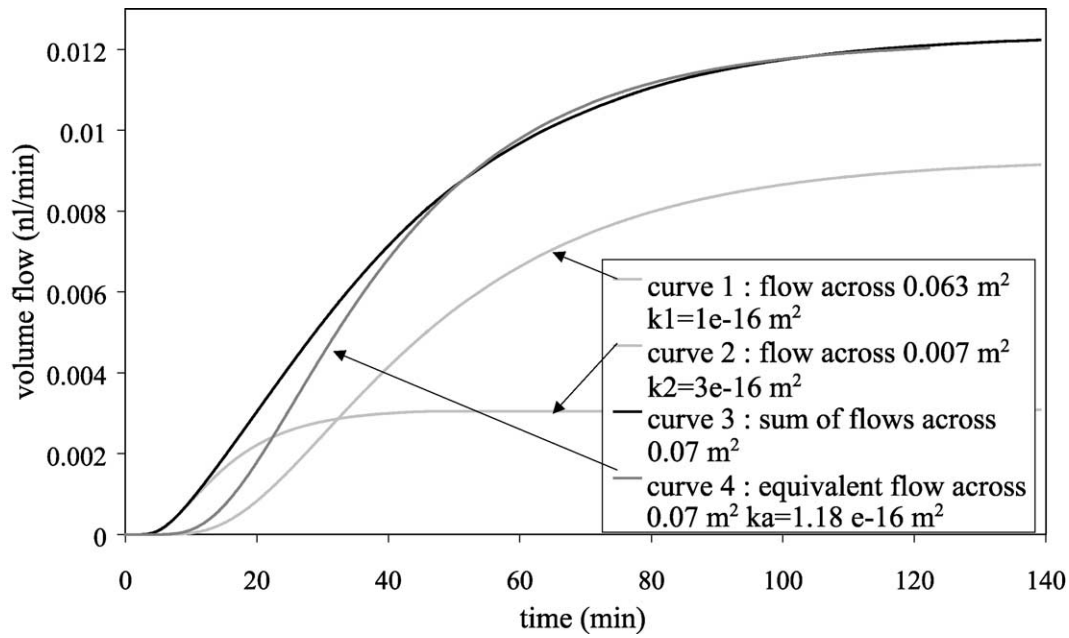

Fig. 7. Percolation effect on flow kinetics for a 0.1-MPa pressure gradient.

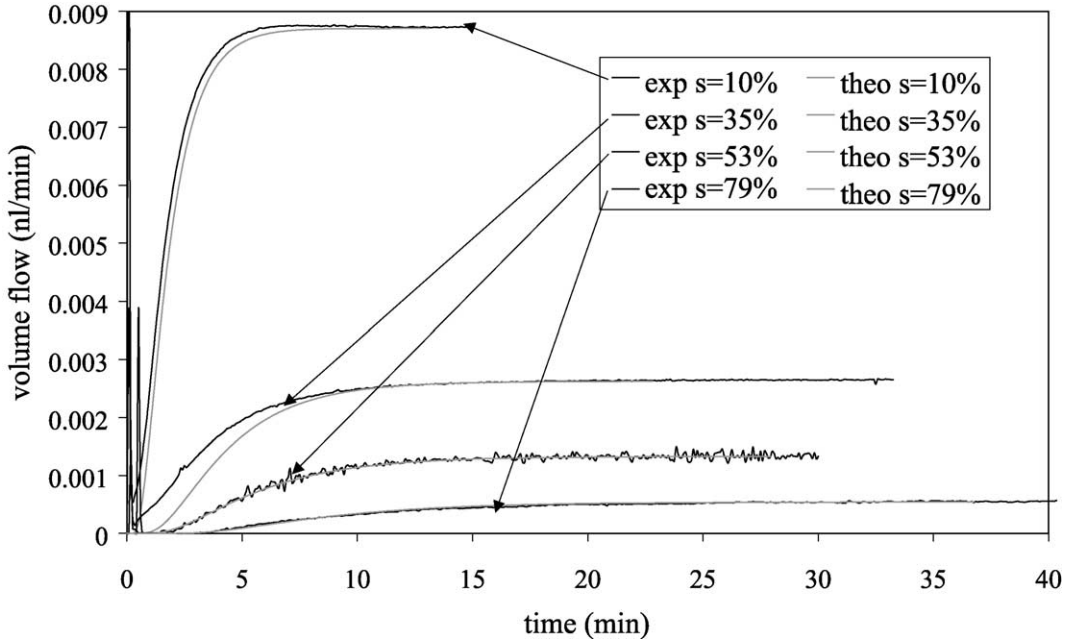

Fig. 8. ϕ 15×5 cm samples with homogeneous water content. Flow kinetics for a 0.1-MPa pressure gradient.

of a sample without distinction of its preferential flow paths. The permeability value only takes on a signification in the steady state. This remark explains the difference between the flow kinetics of Fig. 6.

6.3. Wet samples

Finally, we validated the model for any degree of water saturation with a uniform water content profile. We simulated tests using relative permeability results on ϕ 15×5 cm samples and by evaluating the attainable porosity. Some results are shown in Fig. 8, but all simulations performed gave good correlation between experiment and theory. Depending on the porosity and saturation degree estimations, the flow kinetics were representative to a greater or lesser degree. Permeability measurement in these water content conditions is a particular case of the measurement made on dry samples. Indeed, for wet samples, the attainable gas porosity and flow paths are reduced, but the apparent permeability value takes this into account and allows the experiment to be reproduced.

7. Conclusion

This paper forms part of a study dealing with the evolution of the leakage rate through internal containment walls of nuclear power plants in site test conditions. We attempted to reproduce the concrete as it is found on site in order to transpose our laboratory results. For this, we had to verify that the laws governing fluid transport in porous media were valid for all thickness values. A statistical approach enabled us to conclude that there is no size effect on permeability. Thus, laboratory results can be applied to site. Afterwards, we worked on the TRSS because of its importance in a test in situ. Indeed, to estimate the flows leaving the vessel during a test, we must be sure of the steady state. Moreover, in a test in situ, leakage rate is estimated by internal parameters. If the steady state is not reached, then mass flow leaving the enclosure upstream is higher than the outside one. Thus, leakage rate is over estimated. We have seen that we are able to simulate a head pressure test in order to estimate downstream flows and TRSS for a homogeneous degree of saturation. Therefore, walls are subject to a drying process and their water saturation is heterogeneous (parabolic profile). In this case, a knowledge of the concrete characteristics like attainable porosity and different permeability zones will allow an in situ test to be reproduced as far as gas transfer is concerned.

Acknowledgments

Financial support was provided by The “Centre d’Ingénierie Générale” of Electricité De France. We would like to thank Guy Pastor and Jean Pierre Giraud, our industrial partners and Dr. Mejdi Azaïez from the “Laboratoire de mécanique des fluides de l’Université Paul Sabatier de Toulouse” for his help in the numerical approach.

References

[1] T.C. Powers, Capillary continuity or discontinuity in cement pastes, J. PCA Res. Dev. Lab. 1 (1959) 38–48.
[2] M.P. Yssorche, L’autodessiccation des BHP et BTHP remet elle en

cause leur durabilité? AUGC, Prix jeunes chercheurs René Houpert, Ed. Ecole Centrale Nantes, Nantes, 17–18 Mai, 1995, pp. 247–254.
[3] AFPC-AFREM, Durabilité des bétons—Méthodes recommandées pour la mesure des grandeurs associées à la durabilité, Ed. LMDC, Toulouse, 1996, 283 pp.
[4] A. Abbas, Ecoulements gazeux dans les bétons partiellement saturés: Application à la mesure de perméabilité, PhD thesis, INSA Toulouse, 1998, 154 pp.
[5] M.P. Yssorche, M. Massat, J.P. Ollivier, Micro-cracking analysis of permeability specimens in high performance concrete, Proceedings of the fourth Euroseminar on Microscopy Applied to Building Materials, Visby, Sweden, 1993.
[6] J.J. Kollek, The determination of the permeability of concrete to oxygen by the Cembureau method—a recommendation, Mater. Struct. 22 (1989) 225–230.
[7] D. Perraton, P.C. Aïtcin, A. Carles Gibergues, Mesure de la perméabilité au gaz des bétons: Partie 2. Etude de l'influence de la taille des éprouvettes et de la variabilité des résultats dans le cas d'un BHP, Bull LCPC 221 (1999) 69–87.
[8] A. Abbas, M. Carcassès, J.P. Ollivier, Gas permeability of concrete in relation to its degree of saturation, Mater. Struct. 32 (1999) 3–8.
[9] P. Tassi, Méthodes statistiques, Ed. Economica, Paris, 1989, 474 pp.
[10] A.J. Rossman, Workshop Statistics: Discovery with Data, Springer, New York, 1996, 452 pp.
[11] C. Moyne, Transferts couplés de chaleur et de masse lors du séchage: Prise en compte du mouvement de phase gazeuse, PhD thesis, INP de Lorraine, France, 1987, 293 pp.
[12] W.M. Rohsenow, J.P. Haertnett, E.N. Ganic, Handbook of Heat Transfer Fundamentals, 2nd ed., Mc Graw-Hill, New York, 1985, 1440 pp.